Wind-Driven Residual Currents over a Coastal Canyon

D.B. Haidvogel

Institute of Marine and Coastal Sciences, Rutgers University, P.O. Box 231, New Brunswick, NJ 08903-0231, USA

A. Beckmann

Alfred Wegener Institute for Polar and Marine Research, Am Handelshafen 12, D-27570 Bremerhaven, F.R.Germany

Abstract. Systematic form stress forces can drive mean currents of observable magnitude in the coastal ocean; however, the resulting mean momentum balances are non-linear and solutions, even to simplified form stress problems, must be obtained numerically. Here we ask: what time-mean circulation patterns are produced by an oscillatory wind stress in a coastal ocean featuring a steep coastal canyon intersecting an otherwise smoothly varying continental shelf/slope? Five coastal models of differing algorithmic design are asked to provide answers to this question. If the coastal ocean is homogeneous, the five models give qualitatively similar results—i.e., residual circulation in the sense of intrinsic shelf wave propagation; however, the results are in quantitative disagreement by almost an order of magnitude. If the coastal ocean is stratified, the models are also in qualitative disagreement. Two factors which appear related to these disparities are model vertical coordinate and subgridscale parameterization.

Introduction

Both simplified numerical process studies and statistical mechanical considerations suggest that topographic form stress may contribute significantly to the maintenance of the observed time-mean circulations on and near continental shelves (Haidvogel and Brink, 1986; Holloway et al., 1989). Here we explore the effects of form stress in a topographically irregular coastal channel driven by a time-varying, along-channel wind stress. The topographic irregularity is provided by a steep, cross-shelf canyon, superimposed on a smooth continental shelf/slope profile.

Because non-linearity is important, solutions to the form stress problem are sought numerically using several readily available coastal models. The models include at least one drawn from each vertical coordinate model class (z, sigma, isopycnal). Both low- and high-order numerical algorithms are represented among those tested. The models include the well-known Geophysical Fluid Dynamics Laboratory Modular Ocean Model (GFDLM; Bryan, 1969; Cox, 1984), the Miami Isopycnic Coordinate Ocean Model (MICOM; Bleck et al., 1992), the Princeton Ocean Model (POM; Blumberg and Mellor, 1987), the Spectral Element Model of Iskandarani and colleagues (SEM; Iskandarani et al., 1995), and the SPEM model (Haidvogel et al., 1991; Hedstrom, 1994).

A schematic diagram of the experimental configuration is shown in Figure 1. The geometry is annular, that is, a coastal channel periodic in the x direction, bounded by two (inshore and offshore) walls. The channel dimensions are L_x = 128 × L_y = 96 km. The topography is a continental shelf increasing in depth with cross channel distance intersected by an isolated and idealized canyon:

$$h(x,y) = H_{min} + \frac{1}{2}(H_{max} - H_{min}) \cdot (1 + \tanh(y - Y_c / L_s))$$

with

$$Y_c = Y_0 - L_c \sin^{24}(\pi x / L_x)$$

and H_{min} = 20 m, H_{max} = 4000 m, Y_0 = 32 km, L_s = 10 km, and L_c = 16 km. The resulting topography is both tall (20 m to 4000 m) and steep (maximum slope 30%).

The circulation in the coastal channel is driven by an along-shore wind stress, applied as a body force acting uniformly over the water column:

$$\tau^x = \tau_o \cdot \frac{1}{2}(1 - \tanh((y - \frac{1}{2}L_y)/L_w))$$

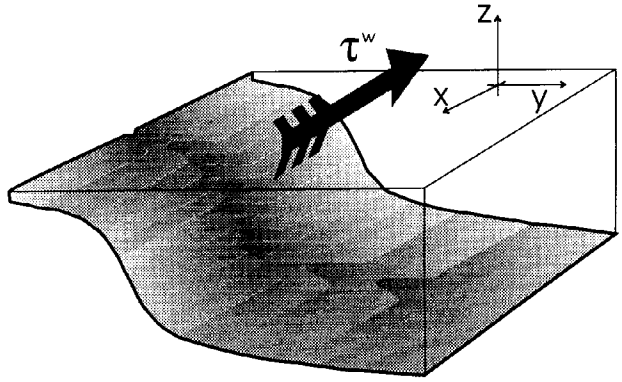

Figure 1. Schematic diagram of the coastal canyon.

with a periodically varying amplitude of

$$\tau_o = 10^{-4} \sin(2\pi t / T_w) \quad \text{Pa kg}^{-1}\text{m}^3$$

with L_w = 10 km and T_w =10 days. Common to all experiments are the constant rate of rotation $f = 1 \cdot 10^{-4}$ m s^{-1}, the gravitational constant $g = 9.81$ m s^{-2}, and a linear bottom stress coefficient $r_B = 3\ 10^{-4}$ m s^{-1}. (Bottom stress is also taken to act uniformly with depth.) Initialized from rest, all runs are carried out to day 120; the last 30 days ($90 < t \leq 120$ days) are averaged to give time-mean fields. Integrations of longer duration (out to day 500) produce slight changes in the time-mean currents; however, the changes are small compared to the differences among individual sets of model results.

Results

The time-mean momentum balance in this fluid system is expected to be intrinsically non-linear (Haidvogel and Brink, 1986). This, together with the deterministic, yet nonetheless complicated, topographic profile, precludes a simple analytic solution. Despite the absence of a known analytical solution, however, we can intercompare the model solutions and assess model-to-model differences. Three bulk measures of model output are discussed here: the maximum pointwise residual (time-mean) current speed at the surface (maximum of $\overline{|\vec{v}(z=0)|}^t$), the maximum residual along-channel averaged current (maximum of $\overline{u}^{xt}$), and the net residual transport through the channel (across-channel integral of $\overline{hu}^{xt}$. These bulk measures are reported for each model in Table 1.

Since the problem as posed is homogeneous, and forced and damped in a depth-independent manner, the flow is expected to remain depth-independent. In principle, therefore, only a single degree of freedom is necessary to represent the vertical structure. Of the models appearing in Table 1, all but one can accommodate the geometry of the coastal channel with a single (or at most a small number of) vertical degrees of freedom. Both the isopycnal and terrain-following models (MICOM, POM, SEM and SPEM) have this capability. The remaining model (GFDLM), being z-coordinate, must represent the irregular topography as a number of steps. Table 1 shows GFDLM results for a total of 10, 20, and 40 levels.

All models require a finite value of lateral viscosity in order to produce smooth, stable results. To insure maximum intercomparability, three of the models (MICOM, SEM and SPEM) have been run with identical sub-gridscale closures (harmonic viscous operators with a constant lateral viscosity coefficient of 5 m^2/s). (Lower values of viscosity produce noisy results in all models.) The GFDLM results were also obtained using a harmonic closure; however, a higher value of viscosity (15 m^2/s) was required for stability. The POM model employed a Smagorinsky formulation (adjustable constant = 0.2). Accompanying these finite values of lateral viscosity, the models are required to impose a lateral boundary condition on horizontal velocity. Since free-slip (no lateral stress) boundary conditions are troublesome to implement on the B-grid GFDLM code, a mixture of free- and no-slip experiments were carried out.

The time step values used in the models (Table 1) roughly reflect the CFL constraints on each. The free sea surface models, with their explicit treatment of surface gravity waves, require quite short time steps, while the two rigid lid models can be run with time step increases of two orders of magnitude.

Table 1. Model intercomparison for the homogeneous form stress experiment.

Model	vertical deg. of freedom	lateral viscosity [m^2/s]	time step [s]	lateral boundary condition	max. $\overline{\lvert\vec{v}(z=0)\rvert}^t$ [cm/s]	max. $\overline{u}^{xt}$ [cm/s]	net transp. [Sv]	comments
GFDLM	40	15	432	no slip	6.7	1.7	0.060	
	20	15	432	no slip	6.9	1.9	0.096	
	10	15	432	no slip	6.0	1.4	0.068	
MICOM	1	5	2	free slip	14.6	3.4	0.231	
	1	5	2	no slip	20.3	1.4	0.142	
POM	5	---	30	free slip	4.6	2.0	0.050	0.2 SM
SEM	1	5	1	free slip	14.6	4.1	0.309	
	1	5	1	no slip	8.7	2.5	0.404	
	1		$\frac{1}{2}$	free slip	16.9	4.2	0.305	$\frac{1}{2}\Delta x$
	1	1	$\frac{1}{2}$	free slip	19.0	4.3	0.231	$\frac{1}{2}$
SPEM	2	5	864	free slip	12.0	3.8	0.250	
	2	5	864	no slip	10.7	3.20	0.240	

Reassuringly, all five models produce residual circulations with the expected overall character—that is, time-mean currents in the sense of intrinsic shelf wave propagation. (We will refer to this direction as "prograde.") Figure 2 shows the resulting curves of $\overline{u}^{xt}$ as a function of cross-shelf distance for five simulations taken from Table 1. All models produce a band of strong prograde residual flow at approximately 10 km offshore. Two of the models (GFDLM and POM) have weak mean retrograde flow further offshore. Residual current vectors (Fig. 3) are largely similar across model classes; slight differences occur in the extent of the recirculation upstream of the canyon (e.g., compare POM and MICOM) and the smoothness of the mean vectors. Note that even with elevated levels of lateral smoothing, GFDLM produces the least smooth of the time-mean currents.

Despite varying degrees of qualitative agreement, the model results differ quantitatively by significant amounts. Maximum pointwise time-mean current speeds vary by a factor of four, and residual transports by a factor of six. The *weakest* currents and lowest overall transports are

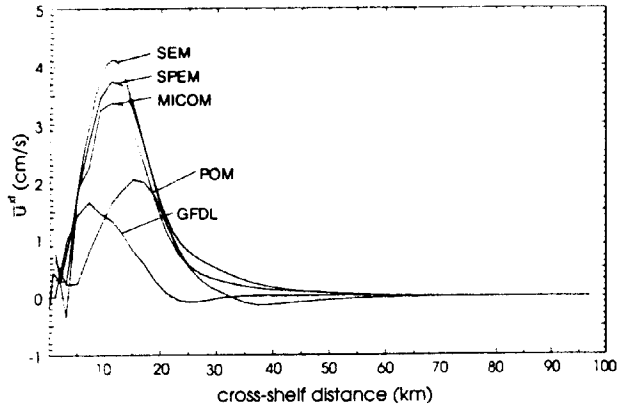

Figure 2. Time- and along-shore mean current $\overline{u}^{xt}$ as a function of cross-shelf distance.

returned by the GFDLM and POM codes. This is likely related in part to the use of a higher value of lateral viscosity in GFDLM and to the Smagorinsky formulation in POM. (Both of these codes produce offshore retrograde flow, which also reduces transport.) Among the free-slip experiments, the *strongest* pointwise residual currents and along-shore transports are found in SEM. Given its high-order formulation, it is tempting to attribute the enhanced strength of the SEM circulation to reduced implicit algorithmic smoothing. Increased horizontal resolution does not result in large changes in any of these model diagnostics, suggesting adequate resolution of all but the inner viscous layer along the coastal wall. Note that the z-coordinate model achieves its highest residual currents with an intermediate number of vertical levels (N=20); increased vertical resolution actually reduces the time-mean circulation. This may indicate incomplete convergence, even with 40 vertical levels.

As might be expected, the introduction of stratification increases model/model differences. Figure 4 (time-mean velocity vectors at a depth of 100 m) shows the outcome of adding a representative vertical stratification to four of the model runs. (Vertical resolution is also increased in each.) This stratified experiment uses a single state variable (density), expressed as a constant (Boussinesq) density (ρ_o) and the initial resting distribution

$$\rho_z = 28.0 - 3.4880 \cdot e^{z/H_\rho} \cdot \left(1.0 - \frac{2}{3}\tanh(z/H_\rho)\right) \sigma\text{ - units}$$

with

$$H_\rho = 800$$

and

$$\rho_o = 1000\ \sigma\text{ - units.}$$

This choice results in a first baroclinic Rossby radius of deformation of 40 km in deepest part of the fluid.

In addition, a vertical viscosity profile is prescribed as

$$\kappa_{uv}(z) = 10 \cdot 10^{-4} + 95 \cdot 10^{-4} \cdot e^{z/H_v} + 95 \cdot 10^{-4} \cdot e^{-z+h(x,y)/H_v}\ \mathrm{m^2 s^{-1}}$$

with $H_v = 50$ m.

The corresponding vertical viscosity is maximum at the top and bottom, and decays into the interior with an e-folding scale of H_v. Finally, in the stratified experiment, surface and bottom stresses are incorporated as boundary conditions at the surface and bottom, respectively.

With stratification, the maximum speed in GFDLM is 2.5 cm/s; there is a broad prograde flow centered at the location of maximum topographic slope, with some intensification at the upstream flank of the canyon. A large anticyclonic feature dominates at the downstream flank of the canyon. The flow is much weaker than in the other models, in part because of the relatively large diffusivity needed for stability. In MICOM, the maximum velocity is 6.3 cm/s; the main prograde current is only weakly influenced by the presence of the canyon. The additional circulation inside the canyon is driven by upwelling motion at the upstream flank and a boundary flow parallel to the depth contours at the downstream side. In contrast to the other models, POM produces a retrograde offshore mean flow, spatially separated from the prograde boundary circulation by a zone of weaker currents. Inside the canyon, the flow is enhanced and cyclonic with a maximum velocity of 7.2 cm/s. Lastly, in SPEM there is an intense boundary current following the depth contours in the canyon area (maximum current 11.7 cm/s), and a prograde off-shore flow that is deflected towards the canyon. At the downstream flank of the canyon,

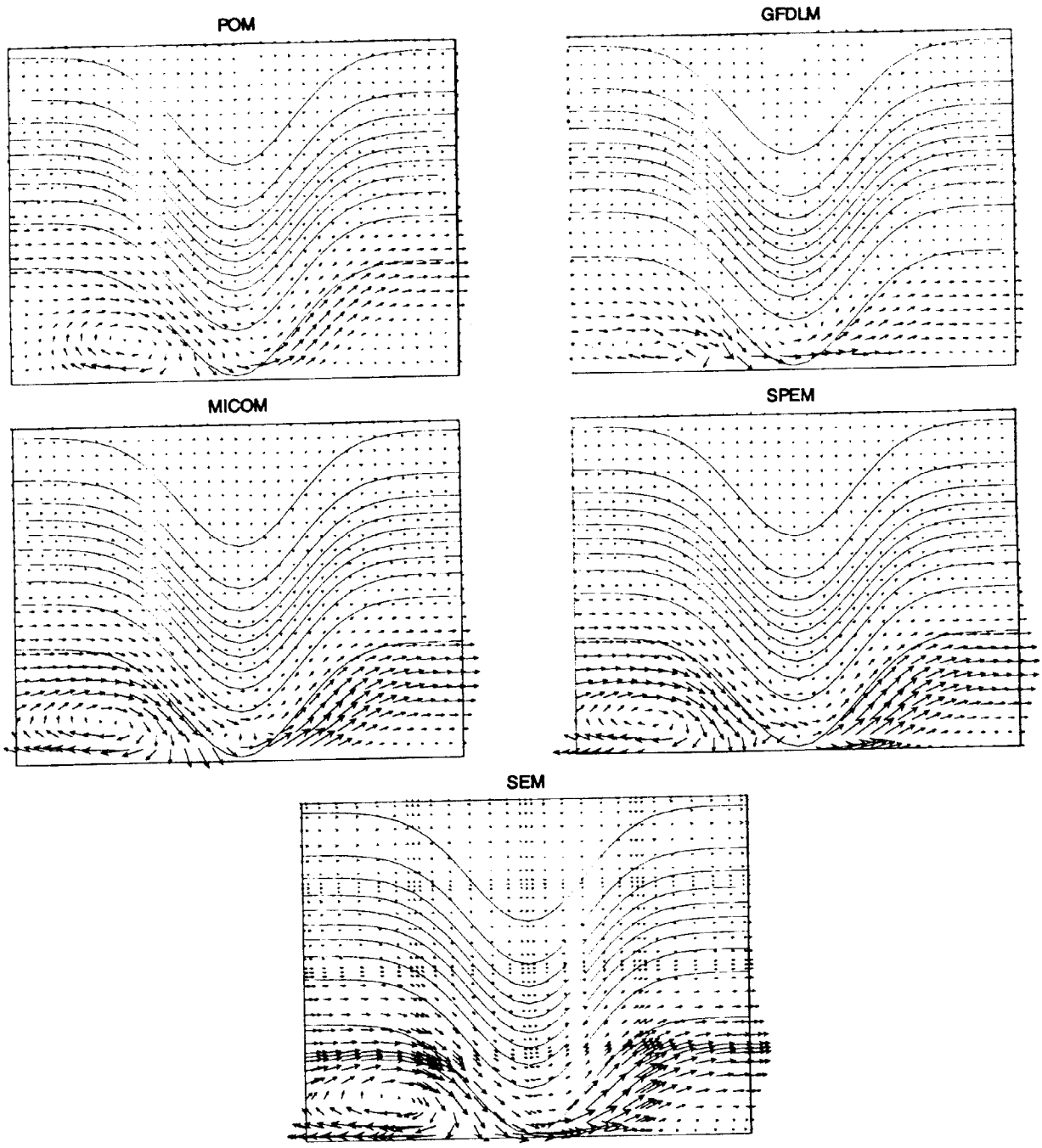

Figure 3. Time-mean surface current vectors for the homogeneous experiment. Maximum vector length is 15 cm s^{-1}. Underlying isobaths are shown (200 m to 3800 m at an interval of 400 m). For clarity, only half of the computational domain is shown in each of the horizontal directions.

pronounced boundary current separation occurs. Undoubtedly, these rather substantial differences reflect a complex interplay between the algorithmic and subgridscale parameterization choices made in each of these models. A more thorough discussion of these intercomparisons is given in Haidvogel and Beckmann (1995).

Interpretation and Discussion

With this single, simple set of intercomparisons, it is of course not possible to unambiguously sort out the respective roles of the many algorithmic differences among the five models employed here. Despite evidence for the impact of higher-order differences in the homogeneous experiment (e.g., SEM gives the strongest

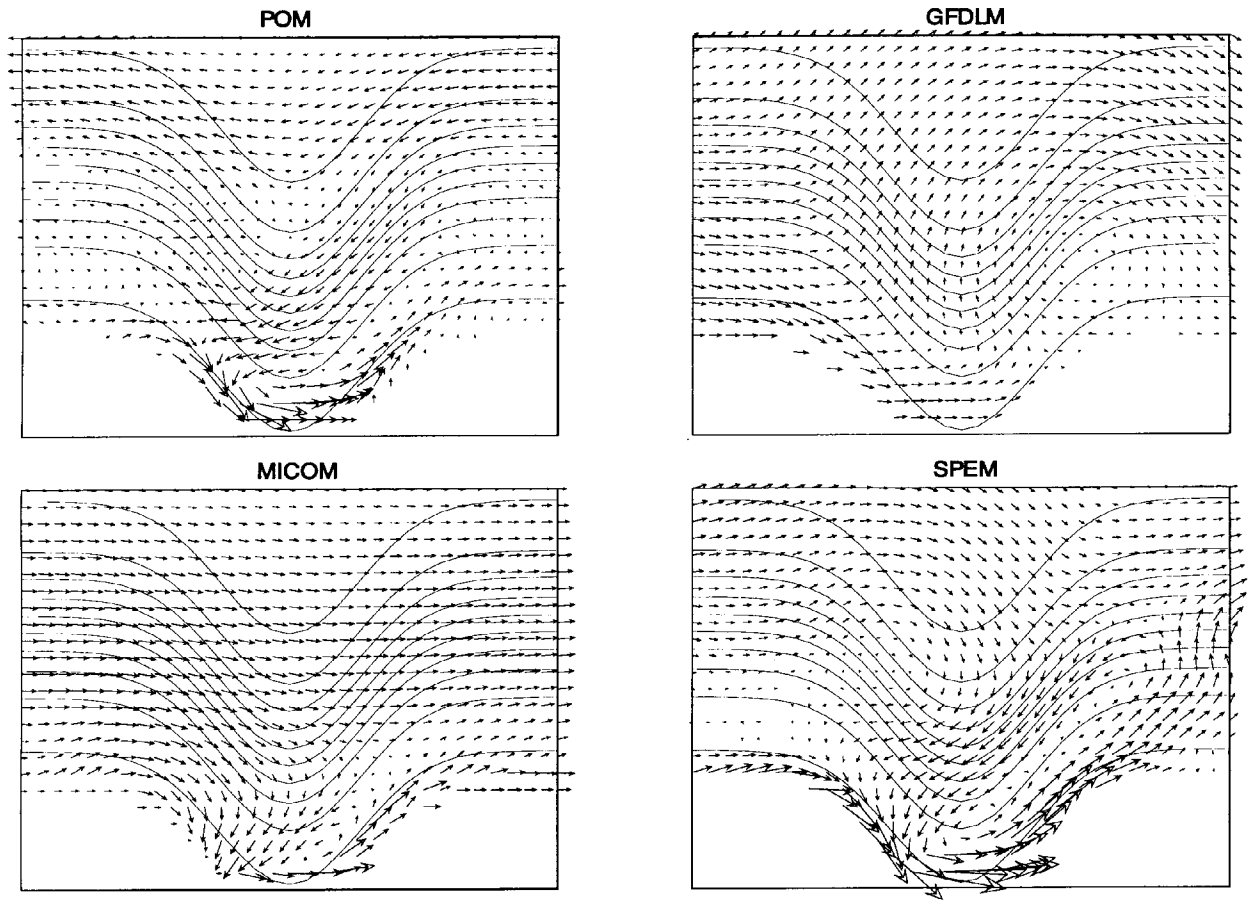

Figure 4. Time-mean current vectors at a depth of 100 m for the stratified problem. Maximum vector length is 12 cm s^{-1} for all models *except* for GFDLM, where 2 cm s^{-1} has been used. Underlying isobaths are shown (200 m to 3800 m at an interval of 400 m). For clarity, only half of the computational domain is shown in each of the horizontal directions.

residual flows), it seems to us that the primary factors involved in determining model differences on these problems are vertical coordinate and subgridscale parameterization.

These two factors are sometimes linked. For example, the requirement for elevated levels of explicit smoothing in the GFDLM code is arguably related to the noise generated in these tests by the stepwise topography. Nonetheless, the precise form of the subgridscale operator is also related to our model results. The POM and SPEM models are rather similar in their algorithmic attributes, except for their use of different subgridscale closures. Even so, they produce rather different pictures of the time-mean flow, particularly in the stratified limit.

The moral of the intercomparison, if any, is that simple numerical test problems such as these may have as much to tell us about our coastal ocean models as they have to say about the coastal ocean.

Acknowledgments

We thank Eric Chassignet, Enrique Curchitser, Mohamed Iskandarani and George Mellor for carrying out some of the intercomparison experiments.

References

Bleck, R., C. Rooth, D. Hu and L. Smith, 1992: Salinity-driven thermocline transients in a wind- and thermohaline-forced isopycnic coordinate model of the North Atlantic, *J. Phys. Oceanogr.* 22 , 1486–1505.

Blumberg, A.F., and G.L. Mellor, 1987: A Description of a three-dimensional coastal ocean circulation model, in Mooers, C. (ed.), Three-dimensional coastal ocean models, *Coastal and Estuarine Sciences*, 4, 1–16.

Bryan, K., 1969: A numerical method for the study of the circulation of the world ocean, *J. Comp. Phys.*, 4 , 347–376.

Cox, M.D., 1984: A primitive equation three-dimensional model of the ocean. Tech. Rep. 1. GFDL Ocean Group, Princeton University, 250 pp.

Haidvogel, D.B., and A. Beckmann, 1995: Numerical modeling of the coastal ocean, *The Sea*, submitted.

Haidvogel, D.B., and K.H. Brink, 1986: Mean currents driven by topographic drag over the continental shelf and slope. *J. Phys. Oceanogr.*, 16, 2159–2171.

Haidvogel, D.B., J.L. Wilkin and R.E. Young, 1991b: A semi-spectral primitive equation ocean circulation model using vertical sigma and orthogonal curvilinear horizontal coordinates, *J. Comp. Phys.*, 94, 151–185.

Hedstrom, K.S., 1994: User's manual for a semi-spectral primitive equation ocean circulation model. Version 3.9, Institute of Marine and Coastal Sciences, Rutgers University, 131 pp.

Holloway, G., K. Brink and D.B. Haidvogel, 1989: Topographic stress in coastal circulation dynamics, in Neshyba, S., et al. (eds.), *Poleward Flows along Eastern Ocean Boundaries*. Coastal and Estuarine Studies, 34, Springer-Verlag, New York, 374 pp.

Iskandarani, M., D.B. Haidvogel and J.P. Boyd, 1995:A staggered spectral element model with applications to the oceanic shallow water equations, *Int. J. Num. Meth. Fluids*, 20, 393–414.